Effect of Hydrofoil Angle of Attack on Resistance Reduction and Lift Generation in a Planing Hull

M. Daffa Nafis Shafwan[1], Kurniawan Teguh Waskito[2*]

(Received: 31 March 2026 / Revised: 6 April 2026 / Accepted: 13 April 2026 / Available Online: 3 June 2026)

***Abstract*—** Hydrodynamic resistance remains a key factor governing the performance of high-speed planing vessels, as it directly determines propulsion power requirements. Despite extensive studies on hydrofoil performance, the application of the NACA 6409 profile in planing hull vessels remains limited. In particular, its potential as a fixed hydrofoil configuration, which may reduce design complexity and enhance practical implementation, has not been thoroughly investigated. Therefore, this study aims to evaluate the effect of hydrofoil angle of attack on resistance reduction and lift generation in a small planing hull vessel. Numerical simulations were conducted using Computational Fluid Dynamics (CFD) in ANSYS Fluent with the SST k–ω turbulence model. Angles of attack of 0°, 5°, 10°, and 15° were analyzed at operating speeds of 15 and 20 knots under foilborne conditions. The results show that low angles of attack, particularly 0° and 5°, provide the greatest resistance reduction, achieving up to 63.3% lower total resistance compared to the non-hydrofoil configuration at 20 knots. In contrast, higher angles of attack (≥10°) increase resistance due to induced drag and flow separation. The hydrofoil configuration also reduces propulsion power requirements and enables foilborne operation at speeds above 15 knots with a minimum angle of attack of 5°. These findings identify the optimal operating range of the NACA 6409 hydrofoil and provide practical design guidance for improving the efficiency of hydrofoil-assisted planing vessels.

Keywords—hydrofoil, NACA 6409, angle of attack, resistance reduction, planing hull, computational fluid dynamics

Corresponding Author: waskito@eng.ui.ac.id

I. INTRODUCTION

Hydrodynamic resistance is a key factor affecting the performance and efficiency of high-speed marine vessels, particularly planing hulls. In the semi-planing and planing regimes, complex interactions among viscous drag, wave-making resistance, and pressure distribution strongly influence total resistance and propulsion power. As vessel speed increases, variations in trim, sinkage, and wetted surface area further intensify these effects, making resistance reduction a primary objective in high-speed craft design [1]. Reducing resistance is essential for lowering propulsion power requirements, thereby improving energy efficiency and reducing operating costs [2].

Planing hulls are widely used to improve hydrodynamic efficiency by generating dynamic lift, which reduces wetted surface area and frictional resistance at higher speeds [1]. Previous studies have shown that planing hull configurations can achieve measurable improvements in resistance performance under appropriate operating conditions [3], [4]. However, hull-form optimization alone is often insufficient when substantial additional resistance reduction is required under demanding operating conditions. Therefore, additional strategies are needed to further enhance vessel performance.

One promising strategy is the integration of hydrofoils. By generating lift, hydrofoils can partially or fully raise the hull above the water surface, thereby reducing wetted area and viscous resistance. Previous studies have demonstrated that properly designed hydrofoils can significantly improve the resistance performance of planing craft, and that their effectiveness is strongly influenced by design and installation parameters such as span, angle of attack, installation height, and foil position [5], [6], [7]. In addition, hydrofoil-assisted configurations have shown considerable potential for improving energy efficiency in high-speed marine transportation [8].

In many advanced applications, hydrofoil systems rely on active or adjustable control mechanisms to maintain stable and efficient operation under varying conditions. In foiling mode, hydrofoil craft are often inherently unstable and generally require control systems to regulate vessel attitude and height [3]. Although effective, such systems introduce additional sensing, actuation, and control requirements, which increase system complexity and may complicate practical implementation. In contrast, fixed hydrofoil configurations offer a simpler and more practical alternative due to their lower complexity and ease of implementation [4]. However, their performance depends strongly on the ability of the hydrofoil profile to generate sufficient lift within a limited angle-of-attack range, since no active control mechanism is available.

Despite extensive research on hydrofoil performance, most existing studies focus on commonly used profiles, generalized foil geometries, or predefined hydrofoil configurations [6], [4]. In planing craft

M. Daffa Nafis Shafwan is with the Department of Mechanical Engineering, Universitas Indonesia, 16424 Depok, Indonesia. Email: m.daffa52@ui.ac.id

Kurniawan Teguh Waskito is with the Department of Mechanical Engineering, Universitas Indonesia, 16424 Depok, Indonesia. Email: waskito@eng.ui.ac.id

applications, previous work has mainly examined the effects of hydrofoil position, angle of attack, span, and submergence on resistance and motion characteristics rather than the hydrodynamic behavior of specific foil profiles [5], [6], [7]. Moreover, flow separation and stall behavior remain critical limitations at higher angles of attack. For instance, studies on the NACA 634-021 profile have shown that wave–foil interaction near the free surface can delay flow separation under certain conditions; however, such effects are highly dependent on the operating environment and are not consistently maintained in practical applications [9]. Consequently, it remains unclear whether a specific hydrofoil profile can consistently generate sufficient lift and maintain a favorable lift-to-drag ratio at relatively low angles of attack, particularly in planing hull applications where passive (fixed) hydrofoil systems are employed. Furthermore, most existing studies primarily focus on fully submerged or actively controlled hydrofoils, leaving a gap in the understanding of passive hydrofoil performance in planing hull configurations.

To address this gap, the NACA 6409 profile is identified as a potential candidate for fixed-hydrofoil applications, given its classification within the NACA 6-series, which is optimized for favorable pressure distribution and reduced drag. Despite these characteristics, its hydrodynamic performance in planing-hull configurations has not yet been systematically evaluated.

Among the governing parameters, the angle of attack plays a critical role as it directly controls lift generation and significantly influences drag behavior. At relatively low angles of attack, a hydrofoil may achieve sufficient lift with a favorable lift-to-drag ratio, which is desirable for efficient operation. However, increasing the angle of attack does not necessarily lead to improved performance, as drag may increase substantially due to enhanced pressure effects, induced drag, and potential flow separation. At higher angles, stall-related phenomena may occur, leading to a degradation in lift and an increase in total resistance. Therefore, selecting an appropriate angle of attack requires careful evaluation of the trade-off between lift generation and resistance characteristics, particularly for fixed hydrofoil systems with limited operational flexibility.

Therefore, this study investigates the effect of angle of attack on the hydrodynamic performance of a NACA 6409 hydrofoil applied to a planing hull using Computational Fluid Dynamics (CFD) simulations in ANSYS Fluent. The analysis is conducted at operating speeds of 15 and 20 knots with angle-of-attack variations of 0°, 5°, 10°, and 15°. The objective is to evaluate the lift, drag, and resistance characteristics of the NACA 6409 profile and to assess its suitability for fixed-hydrofoil planing-hull applications at relatively low angles of attack.

The novelty of this study lies in the integrated hydrodynamic evaluation of the NACA 6409 profile within a planing hull configuration, with particular emphasis on its performance under low-angle, fixed-hydrofoil conditions. The findings are expected to support the development of simpler, more robust, and cost-effective design strategies for hydrofoil-assisted high-speed vessels by reducing reliance on active control systems.

II. Theoretical Background and Formulation

This section presents the theoretical background and formulation relevant to hydrofoil hydrodynamics, planing hull resistance, and the Computational Fluid Dynamics (CFD) approach adopted in the present study. Emphasis is placed on the hydrodynamic role of the hydrofoil in modifying the force balance of a planing hull, particularly through lift generation and its influence on hull resistance. The fundamental principles of hydrofoil lift and drag are first outlined, followed by the analytical characterization of hull resistance using the Slender Body method as a reference. The numerical framework based on the SST k–ω turbulence model in ANSYS Fluent is then introduced as the basis for evaluating hydrofoil lift and the associated resistance reduction of the vessel. These formulations provide the foundation for the subsequent analysis of the hydrodynamic effect of fixed hydrofoil angles of attack on the performance of the planing hull.

Hydrofoil angle of attack (AOA) is one of the principal parameters governing hydrofoil hydrodynamics, as it directly affects the pressure distribution over the foil and hence the generated lift and drag [10], [11], [12]. For a hydrofoil-assisted planing hull, the resulting lift may reduce hull immersion, wetted surface area, and running trim, which in turn may contribute to resistance reduction [13]. However, an increase in AOA does not necessarily lead to superior overall performance, since the associated gain in lift may be accompanied by additional drag and possible flow separation [10], [12], [13]. Accordingly, the hydrodynamic effect of AOA should be assessed on the basis of the balance between lift generation and drag penalty. In the present study, several fixed angles of attack are therefore considered to determine the most favorable operating angle for the selected NACA 6409 hydrofoil under the investigated planing hull condition.

A. Lift and Drag Force Model

In the hydrodynamic analysis of a hydrofoil, the fundamental forces acting on the body are lift $(F_L)$and drag (F_D). These forces arise from the interaction between the hydrofoil surface and the surrounding fluid flow. The magnitudes of these forces are conventionally expressed in terms of the dimensionless lift coefficient $(C_L)$and drag coefficient (C_D)through the following equations [14]:

$$F_L = \frac{1}{2} C_L \cdot \rho \cdot v^2 \cdot A \tag{1}$$

$$F_D = \frac{1}{2} C_D \cdot \rho \cdot v^2 \cdot A \tag{2}$$

In this study, the values of $C_L$and $C_D$were obtained from CFD simulations by integrating the pressure and shear stress distributions over the hydrofoil surface. The hydrodynamic efficiency of the hydrofoil is evaluated by its lift-to-drag ratio (C_L/C_D), which represents the ability of the foil to generate lift with minimum drag penalty.

Furthermore, the foilborne condition, in which the ship hull is fully lifted from the water surface, is achieved when the hydrofoil lift is at least equal to the total ship weight (W), as expressed by:

$$F_L \geq W \tag{3}$$

Satisfying this criterion represents the fundamental condition for foilborne operation and provides a useful reference for evaluating the lift capability of the hydrofoil in the present study.

B. Hull Resistance Analysis

In this study, the Slender Body approach was applied to the bare hull configuration in order to obtain a baseline estimation of ship resistance. This choice is consistent with Michell's wave theory, which is formulated for slender hulls without appendages under steady inviscid flow assumptions [15] [16]. Under these conditions, wave resistance becomes the dominant component of total resistance at Froude numbers greater than 0.3 [17]. With a hull length of 5.704 m and a displacement volume of 0.169 m³, the slenderness ratio $L/V^{1/3}$is 10.32, exceeding the minimum threshold of 4.0 for the validity of the Slender Body method [17]. Moreover, at the design speeds of 5–20 kn, the corresponding Froude numbers range from 0.34 to 1.38, confirming that wave resistance dominates the total resistance within the operational range. Therefore, the application of Michell's theory is considered valid for preliminary resistance prediction. These results serve as a benchmark for comparison with CFD simulations of the hull equipped with hydrofoils, where viscous effects and lift-induced modifications are taken into account [18]. The total resistance coefficient is defined as [18]:

$$C_T = (1+k) \cdot C_F + C_R \tag{4}$$

where $k$is the form factor, C_F is the frictional resistance coefficient, and $C_R$is the residual resistance coefficient. The total resistance force is then expressed as [18]:

$$R_T = \frac{1}{2}\rho V^2 S C_T \tag{5}$$

The frictional resistance coefficient is obtained from the ITTC-1957 correlation line [18]:

$$C_F = \frac{0.075}{(log_{10}Re - 2)^2} \tag{6}$$

The residual resistance coefficient is obtained using the Slender Body integral approach [15],[16] :

$$C_R = \frac{R_W}{\frac{1}{2}\rho V^2 S} \tag{7}$$

These equations were implemented numerically using Maxsurf Resistance, which applies Michell's theory based on the hull centerline geometry.

C. Numerical Modelling of Multiphase Flow

The hydrodynamic performance of hydrofoil-assisted vessels is analyzed using CFD, which enables detailed simulation of multiphase flows under free-surface conditions. To represent the interaction between water and air, the Volume of Fluid (VOF) method is applied [19]. This approach has been widely used in hydrofoil and marine applications to capture wave generation and free-surface deformation [20].

The governing equations are derived from the conservation laws of mass, momentum, and volume fraction, and can be written as:

$$\frac{\partial \rho}{\partial t} + \nabla \cdot (\rho U) = 0 \tag{8}$$

$$\frac{\partial (\rho U)}{\partial t} + \nabla \cdot (\rho U U) = -\nabla p + \nabla \cdot \tau + \rho g \tag{9}$$

$$\frac{\partial c_i}{\partial t} + \nabla \cdot (c_i U) = 0 \tag{10}$$

D. Turbulence Model

To close the Reynolds-Averaged Navier–Stokes (RANS) equations, the Shear Stress Transport (SST) k–ω model is adopted. This turbulence model combines the advantages of the standard k–ε and k–ω formulations, allowing accurate predictions both near solid walls and in free-shear regions. Recent studies in marine hydrodynamics have shown that the SST k–ω model provides reliable results for separated flows, cavitation, and wake dynamics around hydrofoils [21]. Accordingly, this model is considered appropriate for the present CFD simulations of hydrofoil-assisted vessels.

E. Grid Convergence Analysis

To ensure mesh independence, a grid convergence analysis was performed using the Grid Convergence Index (GCI) method originally proposed by Roache [22] and later formalized by Celik [23]. Three mesh levels—coarse, medium, and fine—were generated with a constant refinement ratio. Simulation results for each mesh are denoted as F_1(fine), F_2(medium), and F_3(coarse).

The observed order of convergence (p) was calculated using Richardson extrapolation, and the numerical uncertainty was quantified through the GCI with a safety factor of $F_s = 1.25$, as follows:

$$p = \frac{\ln\left(\frac{f_1 - f_2}{f_2 - f_3}\right)}{\ln(r)} \tag{11}$$

$$GCI = \frac{F_s \varepsilon_{21}}{r^p - 1} \tag{12}$$

where ε_{21} is the approximate relative error between the medium and fine grids. The results of the grid convergence analysis are summarized in Table 2.

III. Research Methodology

This section describes the research methodology, which consists of several key stages. First, hydrofoil lift and drag force modeling was conducted to obtain the fundamental hydrodynamic parameters. Hull resistance was then predicted through CFD simulations in ANSYS Fluent and compared against analytical results from Slender Body theory to establish a reliable benchmark. To ensure numerical accuracy, a grid convergence analysis was performed using the Grid Convergence Index (GCI) method. The CFD setup was subsequently validated by comparing simulation results of the NACA 4412 profile with published numerical and experimental data. Finally, the validated methodology was applied to evaluate the hydrodynamic performance of the NACA 6409 hydrofoil under variations of angle of attack and vessel speed.

A. Research Flowchart

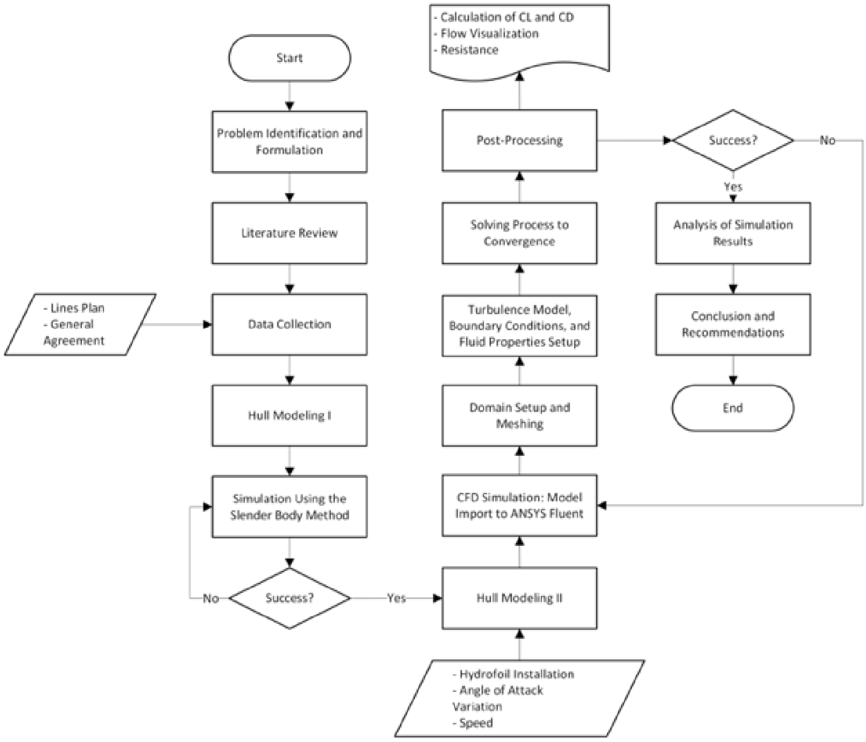

Figure 1. Research flowchart for evaluating the effect of hydrofoil angle of attack on resistance reduction and lift generation

B. Principal Dimensions of the Planing Hull

The data used in this study were obtained from the planing hull developed by the Solar Boat Team Universitas Indonesia. The vessel is equipped with an MPPT (Maximum Power Point Tracking) T50135, which functions to optimize solar energy conversion with a maximum input voltage of 60 V and current of 35 A, and a battery box housing lithium-ion batteries with a total capacity of 48 V–40 Ah.

TABLE 1.
MAIN DIMENSIONS OF THE PLANING HULL

Measurement	Value	Unit
Length Overall (LOA)	5.704	m
cb	0.591	
cp	0.723	
Breadth	0.68	m
Draft	0.086	m
Depth	0.4	m
Design speed	5-20	knots
Displacement	0.1734	t
Froude number (Fn)	1.08-5.42	

The hydrofoil system was designed using a tandem configuration on a planing hull with a total length of 5.704 meters. The hydrofoil has a chord length of 0.1 meter and a span of 0.5 meter. In the tandem configuration, the parameter x represents the distance from the center of gravity (COG) to each foil, which must lie within the range of 0.35L to 0.65L, corresponding to approximately 1.996 to 3.708 meters. To maintain system stability, the distance from the COG to both the forward and aft foils was designed to be equal, resulting in a total span between the two foils of 2x.

The waterline was established at a height of 0.086 meters, with both foils supported by struts measuring 0.331 meters in height. This configuration ensures that the foils remain submerged at an optimal depth. Figure 2 illustrates the final tandem hydrofoil configuration along with its principal dimensions, as applied to the planing hull design.

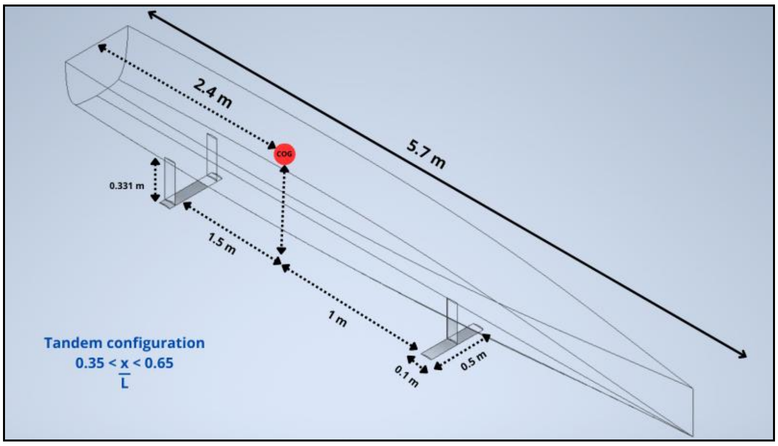

Figure 2. Final design of the planing hull equipped with hydrofoils

C. Numerical Validation

Before simulating the NACA 6409 airfoil, the numerical methodology was validated using the NACA 4412 hydrofoil. This airfoil was selected due to the availability of well-documented reference data, both numerical and experimental. The CFD setup, including mesh strategy, domain configuration, turbulence model, and solver parameters, was kept identical to that used for the NACA 6409 case to ensure consistency and fair comparison with previous studies. Two reference datasets were used for validation: (1) the numerical simulation by Biswas and Harish [24], which employed the SST k−ω turbulence model in a two-dimensional domain with a chord length of 0.1 m and a free-stream velocity of 18.3 m/s, and (2) the towing tank experiment by Kermeen [25], conducted at a velocity of 14.63 m/s with the same chord length of 0.1 m. The computed lift coefficient from the present study showed good agreement with both reference sources, confirming that the adopted numerical approach is reliable and suitable for subsequent analysis of the NACA 6409 hydrofoil.

D. Simulation Setup

In this simulation, which combines the hull and hydrofoil, a half-domain model was employed because the vessel's geometry is symmetric with respect to the center plane. This approach significantly reduces computational cost while maintaining the accuracy of the predicted flow field. According to the ITTC Practical Guidelines for Ship CFD, when geometry and flow are symmetric about a plane, a symmetry boundary may be applied at the centerline to halve the computational domain.

The computational domain was constructed as a three-dimensional rectangular block with a total length of 5.5 L, a width of 1.5 L, and a total height of 2.5 L (comprising 1 L above and 1.5 L below the free surface), where L represents the characteristic length of the hull. The velocity inlet was located 1.5 L upstream of the bow, and the pressure outlet was positioned 3 L downstream of the stern. The top, bottom, and side boundaries were defined as symmetrical planes, while the hull and hydrofoil surfaces were treated as wall boundaries (no-slip condition). A symmetry boundary condition was also applied along the model's centerline to represent the mirrored half of the vessel, as illustrated in Figure 3.

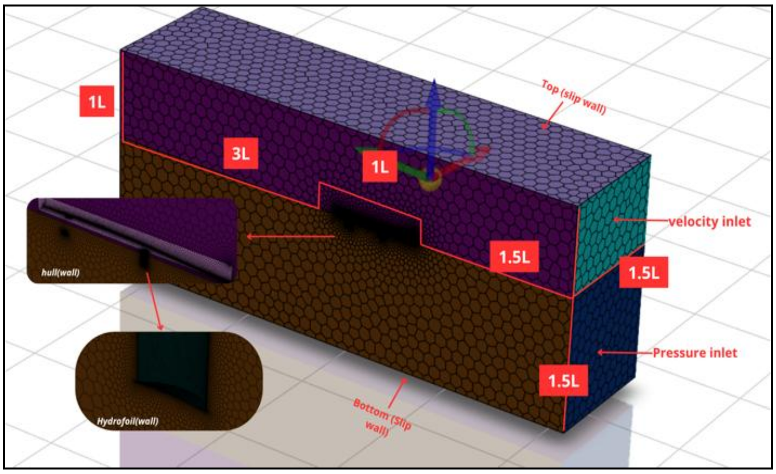

Figure 3. Computational Model of the Planing Hull with Hydrofoil

The computational domain was defined to minimize boundary-induced effects on the flow around the hull and hydrofoil. The inlet and outer boundaries were placed sufficiently far from the body to prevent artificial distortion of the flow field, while the domain depth beneath the hull provided adequate clearance for the hydrofoil and avoided interaction with the lower boundary.

Mesh quality was evaluated in terms of skewness and orthogonal quality, indicating that the generated mesh met the criteria required for reliable numerical analysis. Inflation layers were applied in the vicinity of the hull and hydrofoil surfaces, with a target y^+ value of approximately 1, in order to resolve the boundary layer adequately. Therefore, the mesh was deemed suitable for two-phase flow simulation using the Volume of Fluid (VOF) approach coupled with the $k–\omega$ SST turbulence model.

IV. RESULTS AND DISCUSSION

A. Validation results

The validation results demonstrate that the adopted numerical configuration was capable of accurately reproducing the aerodynamic performance of the NACA 4412 airfoil. The computed lift coefficient (CL) was found to be in close agreement with the numerical results reported by Biswas and Harish [24] and the experimental data reported by Kermeen [25], as illustrated in Figure 4. These findings confirm the reliability of the selected SST k–ω turbulence model and the overall numerical methodology, thereby supporting their application in the subsequent simulation of the NACA 6409 hydrofoil.

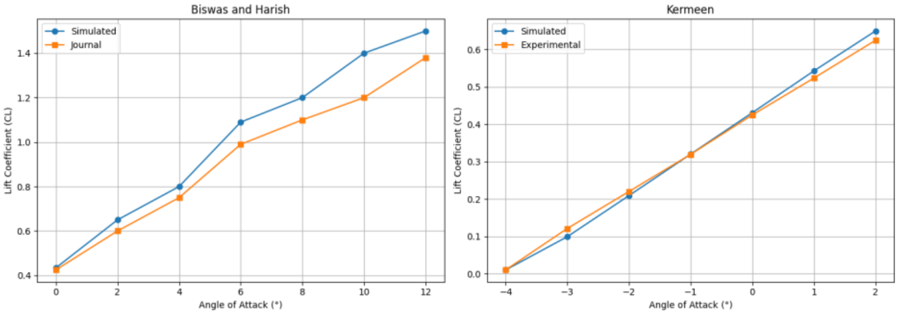

Figure 4. Comparison of simulated lift coefficient (CL) with reference data from Biswas and Harish [24] and Kermeen [25].

B. Simulation Results of the NACA 6409 Hydrofoil

Before conducting the main analysis of the NACA 6409 hydrofoil, a grid independence test was performed to ensure that the numerical results were not significantly affected by mesh density. The Grid Convergence Index (GCI) method was employed to evaluate the convergence level of the solution with respect to mesh refinement. Three grid resolutions—coarse, medium, and fine—were tested, with the corresponding number of elements listed in Table 2.

The mesh configurations for each grid level are illustrated in Figure 5, where (a) represents the fine mesh, (b) the medium mesh, and (c) the coarse mesh.

TABLE 2.
GRID RESOLUTIONS USED IN THE GRID INDEPENDENCE TEST

Grid Level	Number of Elements (N)	CL Value
Coarse	9.114	0.647
Medium	172.892	0.654
Fine	675.188	0.652

(a)

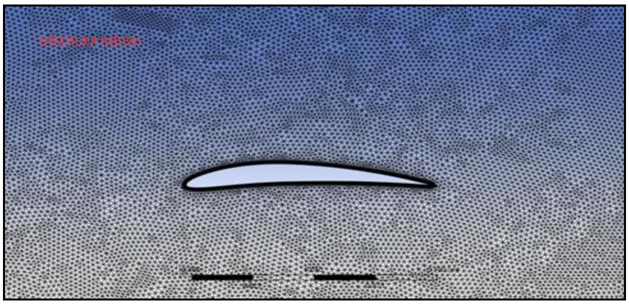

(b)

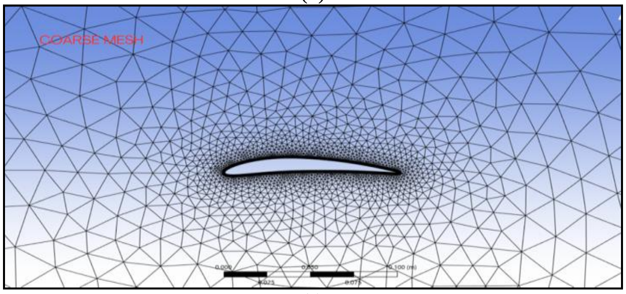

(c)

Figure 5. Mesh configurations of the NACA 6409 hydrofoil: (a) fine, (b) medium, and (c) coarse grids

C. Grid Convergence Analysis

The quantitative results of the grid convergence analysis, including the convergence order (p), approximate relative error (ε_{21}), and GCI values, are summarized in Table 3.

TABLE 3.
GRID CONVERGENCE ANALYSIS RESULTS

Parameter	Value
Order of convergence (p)	0.851
Exact solution (Richardson extrapolation)	0.65120
Approximate relative error (ε_{21})	0.307%
Grid Convergence Index (GCI) – fine grid	0.153%

The obtained convergence order $p = 0.851$, indicates that the solution lies within the range of monotonic convergence. The low GCI value (<1%) for the fine grid demonstrates that the numerical results are sufficiently converged and independent of mesh density variations. Therefore, the fine grid with a total of 675,188 elements was selected as the baseline mesh for the main simulations of the NACA 6409 hydrofoil.

D. Lift and Drag Coefficients of the NACA 6409 Hydrofoil

The simulation of the NACA 6409 hydrofoil was carried out using the SST k–ω turbulence model with a chord length of 0.1 m and flow velocities ranging from 5 to 20 knots. The results show that the lift coefficient (C_L) increases with the angle of attack (AOA) until reaching the stall point and the drag coefficient (C_D) gradually increases with AOA and rises sharply after flow separation occurs as shown in Figure 6.

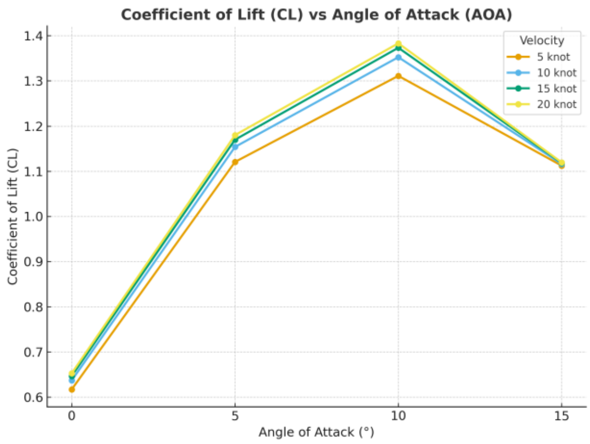

(a)

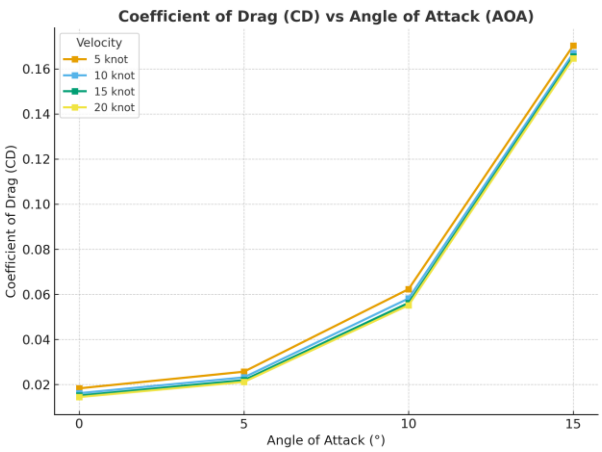

(b)

Figure 6. (a) Lift coefficient (C_L) versus AOA at various velocities and (b) Drag coefficient (C_D) versus AOA at various velocities

To complement the numerical analysis, the simulation results are visualized through velocity magnitude and static pressure contours to illustrate the flow pattern and pressure distribution around the NACA 6409 profile at various angles of attack. The visualization focuses on two key parameters:

- Velocity Contour**:** Indicates acceleration, deceleration, and potential flow separation.
- Pressure Contour**:** Shows the pressure difference between the upper and lower surfaces related to lift generation.

Visualizations are presented for four main angles of attack (0°, 5°, 10°, and 15°) at a flow velocity of 20 knots (10.28 m/s) representing the maximum condition.

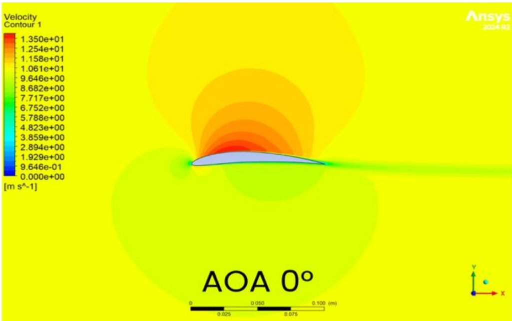

(a)

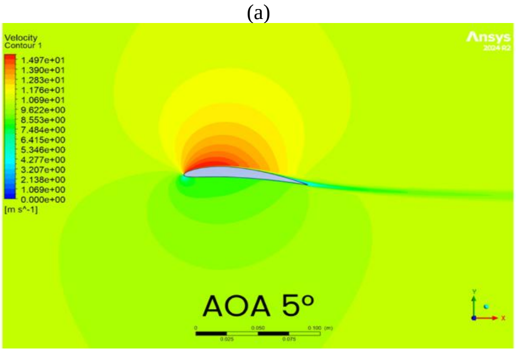

(b)

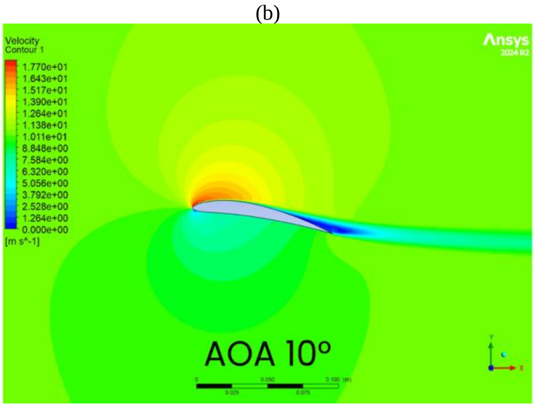

(c)

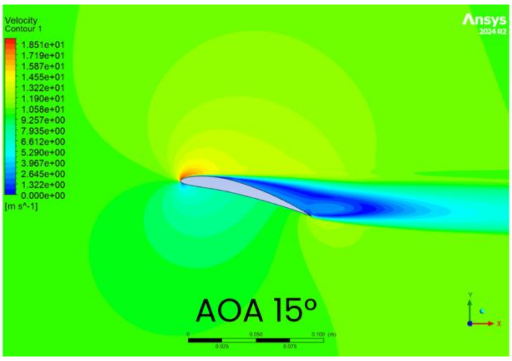

(d)

Figure 7. Velocity contours around the NACA 6409 hydrofoil at different angles of attack: (a) 0°, (b) 5°, (c) 10°, and (d) 15°

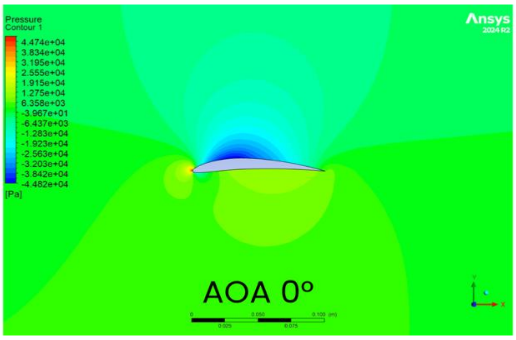

(a)

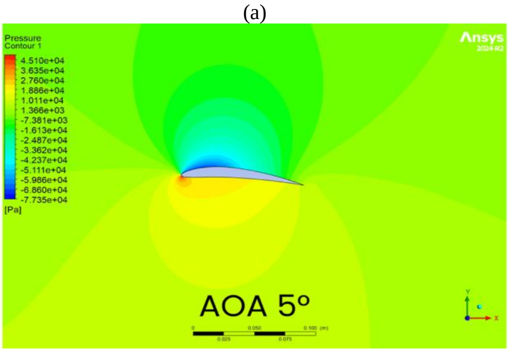

(b)

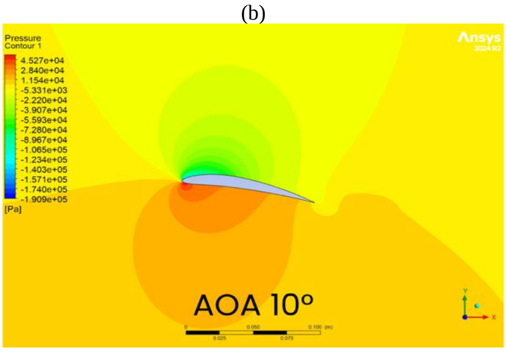

(c)

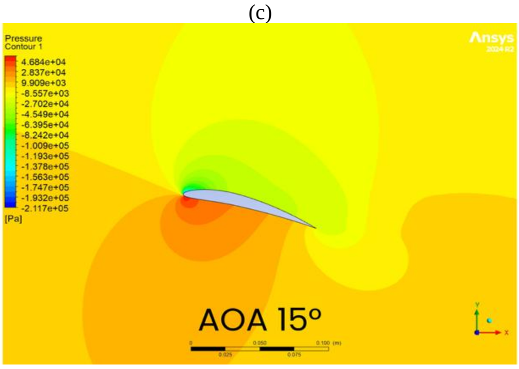

(d)

Figure 8. Pressure contours around the NACA 6409 hydrofoil at different angles of attack: (a) 0°, (b) 5°, (c) 10°, and (d) 15°

The flow visualization shows a nearly symmetric pattern at 0° AOA with minimal lift generation. At 5°, acceleration on the upper surface and a corresponding pressure drop indicate the onset of the Bernoulli effect and increased lift. At 10°, maximum acceleration and the lowest static pressure occur, resulting in the highest lift coefficient with fully attached flow. At 15°, flow separation appears near the upper trailing edge, leading to uneven pressure distribution, reduced lift-to-drag efficiency, and increased drag. These results confirm the numerical analysis and illustrate the transition from stable to stall conditions with increasing angle of attack.

E. Effect of Lift Force on Ship Weight and Draft

After obtaining the lift coefficient (C_L) from the numerical simulation of the NACA 6409 hydrofoil profile, the total lift force generated by the two-hydrofoil configuration was calculated. This lift force was then used to determine the vessel's new effective weight, which was obtained by subtracting the generated lift force from the ship's initial displacement of 1701 N.

Figure 9 presents the comparison between the lift force and the ship's displacement at various angles of attack. The graph illustrates the relationship between lift force and velocity, along with the ship's displacement line. This visualization helps to identify the conditions where the generated lift force exceeds the vessel's displacement, indicating the transition from the hull-borne to the foil-borne state.

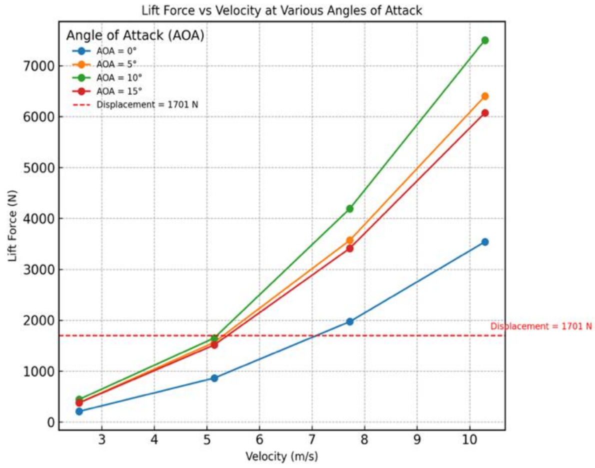

Figure 9. Comparison of Lift Force and Ship Displacement at Various Angles of Attack

The results illustrated in Figure 8 show that at angles of attack (AOA) of 5° or greater and speeds above 7.7 m/s, most configurations achieve a foilborne condition. The hydrofoil configurations with AOA of 10° and 15° exhibit the highest lift effects, whereas the configuration with AOA of 0° requires a significantly higher velocity to reach a similar lift performance.

F. CFD Analysis under Foilborne Conditions

Based on the previous evaluation, further CFD simulations in ANSYS Fluent were focused on foilborne configurations, in which the vessel was fully lifted by the hydrofoils and operated above the water surface. In this regime, the hull–water interaction was minimized, and the flow field primarily consisted of hydrodynamic forces on the hydrofoils and aerodynamic drag on the exposed hull.

The simulations covered four angles of attack (AOA)—0°, 5°, 10°, and 15°—and two operating speeds, 15 knots (7.72 m/s) and 20 knots (10.29 m/s). The main objective was to evaluate how these parameters influenced total drag and required power under foil-borne conditions.

To visualize the results clearly, Figure 10 presents a bar chart comparison of total ship resistance between the slender-body hull and the hydrofoil-assisted configuration for each test case. The results indicate that AOA = 0° and 5° provide substantial drag reduction, reaching up to 63.3% at 20 knots. In contrast, AOA = 10° and 15° result in higher drag, primarily due to increased induced resistance and flow separation on the hydrofoil surfaces.

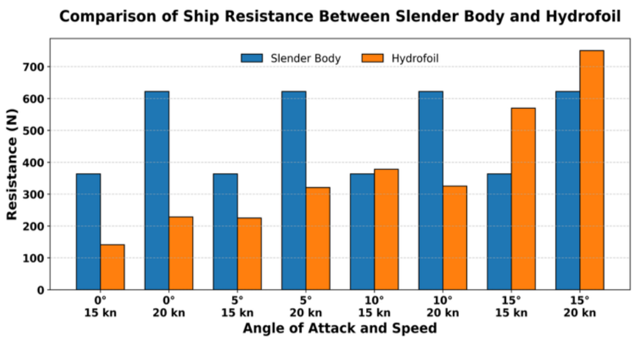

Figure 10. Comparison of ship resistance between slender-body and hydrofoil-assisted configurations

From these resistance results, the corresponding power requirements were estimated, as illustrated in Figure 11. Hydrofoil configurations at low AOAs demonstrate substantial power savings, while higher AOAs lead to a sharp rise in power demand due to increased hydrodynamic resistance.

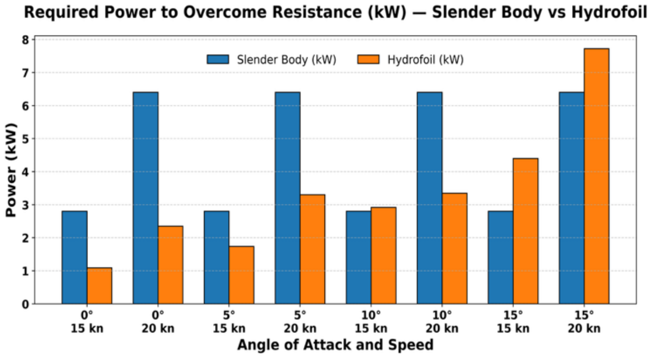

Figure 11. Comparison of ship power requirements.

The AOA = 0° case at 10.28 m/s was selected for detailed flow visualization as it represents the most stable and efficient foilborne condition. The volume-fraction contour of water (Figure 12) shows full hull lift with minimal surface disturbance. The bottom view (subfigure a) reveals uniform lift distribution, while the front view (subfigure b) confirms stable lift generation and symmetric flow.

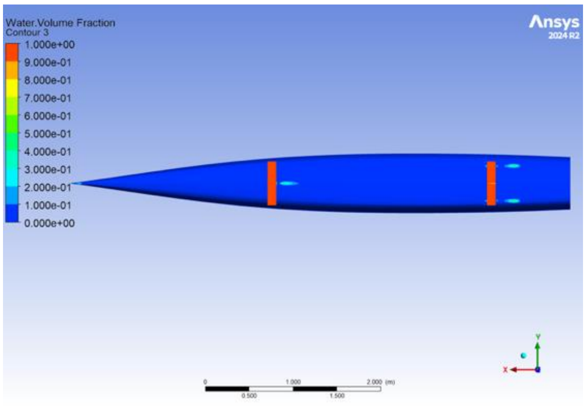

(a)

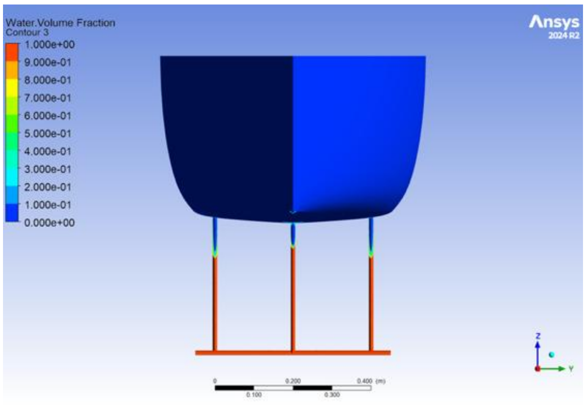

(b)

Figure 12. Volume-fraction contour of water at AOA = 0° and 10.28 m/s: (a) bottom view showing uniform lift; (b) front view indicating stable, symmetric flow.

In contrast, the AOA = 15° case at 10.28 m/s (Figure 13) demonstrates that stronger lift does not always improve performance. The bottom view (subfigure a) exhibits asymmetric flow and vortex formation, and the front view (subfigure b) shows disturbed free-surface patterns, indicating flow separation and increased resistance.

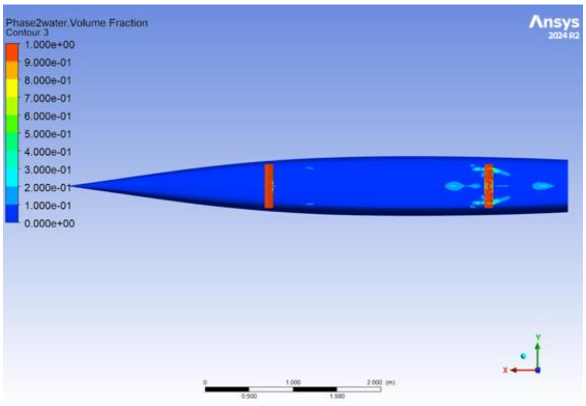

(a)

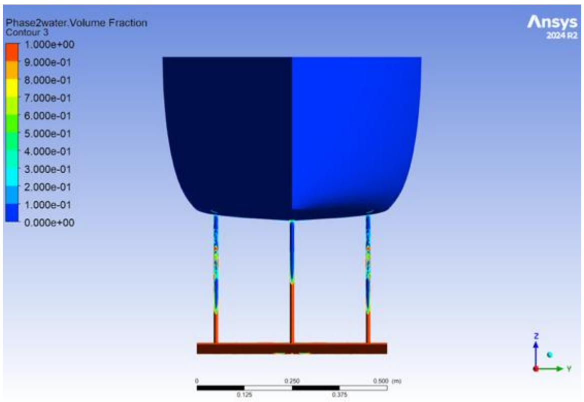

(b)

Figure. 13. Volume-fraction contour of water at AOA = 15° and 10.28 m/s: (a) bottom view showing asymmetric flow and vortices; (b) front view indicating flow separation and higher resistance.

V. CONCLUSION

Based on the numerical simulations and hydrodynamic performance analysis, this study confirms that the angle of attack of the NACA 6409 hydrofoil has a significant influence on the resistance reduction and lift generation of a small planing hull vessel. This finding is consistent with the main objective of the study, which was to evaluate the effect of hydrofoil angle of attack on the hydrodynamic performance of the vessel under foilborne operating conditions.

The results show that low angles of attack, particularly 0° and 5°, provide the most favorable hydrodynamic performance. Under these conditions, the hydrofoil configuration produced the greatest reduction in total resistance, with a maximum decrease of 63.3% compared to the non-hydrofoil configuration at a speed of 20 knots. These results indicate that the NACA 6409 profile performs effectively at relatively low angles of attack, where it is able to reduce drag while maintaining favorable flow characteristics.

In terms of lift generation, the hydrofoil was capable of producing sufficient upward force to support foilborne operation. The transition to a fully foilborne state occurred at speeds above 7.72 m/s (approximately 15 knots) with a minimum angle of attack of 5°, where the tandem hydrofoil configuration generated enough lift to completely raise the hull above the water surface. This demonstrates that the hydrofoil contributes not only to resistance reduction but also to improved vessel efficiency through reduced hull–water interaction.

By contrast, higher angles of attack, namely 10° and 15°, resulted in increased resistance due to induced drag, flow separation, and stall phenomena. Although increasing the angle of attack may enhance lift to a certain extent, excessive angles reduce the overall hydrodynamic efficiency of the vessel. This indicates that the NACA 6409 profile is less suitable for operation at higher angles of attack in fixed-hydrofoil planing hull applications.

Overall, the study concludes that the optimal operating range of the NACA 6409 hydrofoil lies at low angles of attack, especially between 0° and 5°, where resistance reduction and lift generation can be effectively balanced. Therefore, the NACA 6409 profile can be considered a promising option for fixed-hydrofoil applications in small planing hull vessels, provided that it operates within an appropriate angle-of-attack range. These findings provide practical guidance for the design of hydrofoil-assisted planing vessels and may serve as a useful reference for further experimental validation and the future development of efficient high-speed craft.

NOMENCLATURE

F_L = Lift force (N)
F_D = Drag force (N)
C_L = Lift coefficient

C_D = Drag coefficient
ρ = Fluid density (kg/m^3)
ν = Flow velocity (m/s)
A = Reference area (m^2)
W = Weight of body (N)
C_F = Frictional resistance coefficient
R_e = Reynolds number
C_R = Residual resistance coefficient
R_W = Wave-making resistance (N)
C_T = Total resistance coefficient
k = Form factor
R_T = Total resistance (N)
S = Wetted surface area (m^2)
t = Time (s)
U = Velocity vector (m/s)
p = Static pressure (Pa)
∇ = Nabla operator
τ = Viscous stress tensor (N/m^2)
g = Gravitational acceleration vector (m/s^2)
c_i = Volume fraction of phase i
$\nabla.$ = Divergence operator
∇p = Pressure gradient (Pa/m)
$\partial/\partial t$ = Partial time derivative
p = Observed order of convergence
f_2 = Numerical result on medium grid
f_3 = Numerical result on coarse grid
r = Grid refinement ratio
GCI = Grid Convergence Index (% or -)
F_s = Safety factor
ε_{21} = Relative error

REFERENCES

[1] S. Tavakoli, M. Zhang, A. A. Kondratenko, and S. Hirdaris, "A review on the hydrodynamics of planing hulls," Jul. 01, 2024, *Elsevier Ltd*. doi: 10.1016/j.oceaneng.2024.117046.

[2] A. Sardar, R. Islam, M. Anantharaman, and V. Garaniya, "Advancements and obstacles in improving the energy efficiency of maritime vessels: A systematic review," May 01, 2025, *Elsevier Ltd*. doi: 10.1016/j.marpolbul.2025.117688.

[3] A. Steinert, A. Hug, P. Medl, T. Schulze, and F. Holzapfel, "Modeling and dynamic analysis of a 'flying' fully submerged hydrofoil craft for control," *Aerospace Systems*, 2026, doi: 10.1007/s42401-025-00445-y.

[4] K. Akbari Vakilabadi, H. R. Ghafari, and H. Ghassemi, "Investigation of front hydrofoil position influence on the hydrofoil-assisted craft," *Ocean Engineering*, vol. 304, Jul. 2024, doi: 10.1016/j.oceaneng.2024.117901.

[5] H. Shen, Q. Xiao, J. Zhou, Y. Su, and X. Bi, "Design of hydrofoil for the resistance improvement of planing boat based on CFD technology," *Ocean Engineering*, vol. 255, Jul. 2022, doi: 10.1016/j.oceaneng.2022.111413.

[6] E. D'Amato, I. Notaro, V. Piscopo, and A. Scamardella, "Hydrodynamic Design of Fixed Hydrofoils for Planing Craft," *J. Mar. Sci. Eng.*, vol. 11, no. 2, Feb. 2023, doi: 10.3390/jmse11020246.

[7] X. Bi, H. Shen, J. Zhou, and Y. Su, "Numerical analysis of the influence of fixed hydrofoil installation position on seakeeping of the planing craft," *Applied Ocean Research*, vol. 90, Sep. 2019, doi: 10.1016/j.apor.2019.101863.

[8] J. M. K. Godø, S. Steen, and O. M. Faltinsen, "A resistance model for hydrofoil fast ferries with fully submerged foil systems," *Ocean Engineering*, vol. 301, Jun. 2024, doi: 10.1016/j.oceaneng.2024.117503.

[9] Z. Ni, M. Dhanak, and T. chow Su, "Performance of a hydrofoil operating close to a free surface over a range of angles of attack," *International Journal of Naval Architecture and Ocean Engineering*, vol. 13, pp. 1–11, Nov. 2021, doi: 10.1016/j.ijnaoe.2020.11.002.

[10] Q. Xiao and W. Liao, "Numerical investigation of angle of attack profile on propulsion performance of an oscillating foil," *Comput. Fluids*, vol. 39, no. 8, pp. 1366–1380, Sep. 2010, doi: 10.1016/j.compfluid.2010.04.006.

[11] G. He *et al.*, "Modification of effective angle of attack on hydrofoil power extraction," *Ocean Engineering*, vol. 240, Nov. 2021, doi: 10.1016/j.oceaneng.2021.109919.

[12] L. Mei, W. Yan, J. Zhou, Y. Tang, and W. Shi, "Angle of Attack Characteristics of Full-Active and Semi-Active Flapping Foil Propulsors," *Water (Switzerland)*, vol. 16, no. 20, Oct. 2024, doi: 10.3390/w16202957.

[13] Z. Ni, M. Dhanak, and T. chow Su, "Performance of a hydrofoil operating close to a free surface over a range of angles of attack," *International Journal of Naval Architecture and Ocean Engineering*, vol. 13, pp. 1–11, Nov. 2021, doi: 10.1016/j.ijnaoe.2020.11.002.

[14] H. Qu, X. Li, and X. Dong, "Numerical Study on Hydrodynamic Performance of a Pitching Hydrofoil with Chordwise and Spanwise Deformation," *J. Mar. Sci. Eng.*, vol. 12, no. 5, May 2024, doi: 10.3390/jmse12050830.

[15] Md. Salim Kamil, M. A. A. Roslan, and M. F. Misran, "Comparative Study of Ship Wave Resistance by Various Methods of Solution," in *Advanced Maritime Technologies and Applications*, A. Ismail, W. M. Dahalan, and A. Öchsner, Eds., Cham: Springer International Publishing, 2022, pp. 121–127.

[16] S. Duman, E. Boulougouris, M. Z. Aung, X. Xu, and A. Nazemian, "Numerical Evaluation of the Wave-Making Resistance of a Zero-Emission Fast Passenger Ferry Operating in Shallow Water by Using the Double-Body Approach," *J. Mar. Sci. Eng.*, vol. 11, no. 1, Jan. 2023, doi: 10.3390/jmse11010187.

[17] C. Guo, X. Zhong, and D. Zhao, "Research on Scale Effect of Resistance Components for Full-Formed Ship Based on Large-Scale Model Towing Test," *J. Mar. Sci. Eng.*, vol. 11, no. 7, Jul. 2023, doi: 10.3390/jmse11071300.

[18] Y. Yang *et al.*, "Research on Ship Resistance Prediction Using Machine Learning with Different Samples," *J. Mar. Sci. Eng.*, vol. 12, no. 4, Apr. 2024, doi: 10.3390/jmse12040556.

[19] C. W. Hirt and B. D. Nichols, "Volume of fluid (VOF) method for the dynamics of free boundaries," *J. Comput. Phys.*, vol. 39, no. 1, pp. 201–225, 1981, doi: https://doi.org/10.1016/0021-9991(81)90145-5.

[20] E. Esmaeilifar, M. Hassan Djavareshkian, B. Forouzi Feshalami, and A. Esmaeili, "Hydrodynamic simulation of an oscillating hydrofoil near free surface in critical unsteady parameter," *Ocean Engineering*, vol. 141, pp. 227–236, 2017, doi: https://doi.org/10.1016/j.oceaneng.2017.06.037.

[21] M. Zhao, D. Wan, and Y. Gao, "Comparative study of different turbulence models for cavitational flows around naca0012 hydrofoil," *J. Mar. Sci. Eng.*, vol. 9, no. 7, Jul. 2021, doi: 10.3390/jmse9070742.

[22] P. J. Roache, "Perspective: A Method for Uniform Reporting of Grid Refinement Studies," *J. Fluids Eng.*, vol. 116, no. 3, pp. 405–413, Sep. 1994, doi: 10.1115/1.2910291.

[23] I. B. Celik, U. Ghia, P. J. Roache, C. J. Freitas, H. Coleman, and P. E. Raad, "Procedure for estimation and reporting of uncertainty due to discretization in CFD applications," *Journal of Fluids Engineering, Transactions of the ASME*, vol. 130, no. 7, pp. 0780011–0780014, Jul. 2008, doi: 10.1115/1.2960953.

[24] S. Biswas and R. Harish, "Effect of unsteady cavitation on hydrodynamic performance of NACA 4412 Hydrofoil with novel triangular slot," *Heliyon*, vol. 11, no. 3, Feb. 2025, doi: 10.1016/j.heliyon.2025.e42266.

[25] R. W. Kermeen, "Naca 4412 and walchner profile 7 hydrofoils in non-cavitating and cavitating flows," *Rep*, vol. 47, pp. 1–21, 1956.